J|A|C|S
ARTICLES
Published on Web 01/21/2006

Spontaneous Fibril Formation by Polyalanines; Discontinuous Molecular Dynamics Simulations

Hung D. Nguyen and Carol K. Hall*

Contribution from the Department of Chemical Engineering, North Carolina State University, Raleigh, North Carolina 27695-7905

Received June 14, 2005; E-mail: hall@turbo.che.ncsu.edu

Abstract: Fibrillary protein aggregates rich in β-sheet structure have been implicated in the pathology of several neurodegenerative diseases. In this work, we investigate the formation of fibrils by performing discontinuous molecular dynamics simulations on systems containing 12 to 96 model $Ac-KA_{14}K-NH_2$ peptides using our newly developed off-lattice, implicit-solvent, intermediate-resolution model, PRIME. We find that, at a low concentration, random-coil peptides assemble into α-helices at low temperatures. At intermediate concentrations, random-coil peptides assemble into α-helices at low temperatures and large β-sheet structures at high temperatures. At high concentrations, the system forms β-sheets over a wide range of temperatures. These assemble into fibrils above a critical temperature which decreases with concentration and exceeds the isolated peptide's folding temperature. At very high temperatures and all concentrations, the system is in a random-coil state. All of these results are in good qualitative agreement with those by Blondelle and co-workers on $Ac-KA_{14}K-NH_2$ peptides. The fibrils observed in our simulations mimic the structural characteristics observed in experiments in terms of the number of sheets formed, the values of the intra- and intersheet separations, and the parallel peptide arrangement within each β-sheet. Finally, we find that when the strength of the hydrophobic interaction between nonpolar side chains is high compared to the strength of hydrogen bonding, amorphous aggregates, rather than fibrillar aggregates, are formed.

Introduction

The assembly of normally soluble proteins into ordered aggregates, known as amyloid fibrils, is a cause or associated symptom of numerous human disorders, including Alzheimer's, the prion diseases, and adult-onset diabetes.[1−5] In each of these disorders, which are known collectively as the amyloidoses, a specific protein slowly accumulates in fibrillar tangles or plaques, destroying the architecture and function of the surrounding tissue, usually with degenerative and ultimately fatal consequences. Although little is known about the molecular basis for fibrillization, tantalizing clues emerge when the common features of the various amyloidoses are examined. Fibrils of amyloidogenic proteins formed in vitro exhibit strikingly similar morphologies despite a lack of similarity in their sequence, structure, and function.[4,6−9] They are invariably long, straight, and unbranched and consist of two or more smaller fibrils, called protofilaments (and sometimes protofibrils) which are themselves long ribbons of layered crossed β-sheets propagating along the fibril axis.[10−15] Recent evidence that proteins other than those associated with amyloid diseases form fibrils in vitro under mildly denaturing conditions[8,9,16−19] has led leaders in the field to suggest that fibril formation is an intrinsic property of polypeptides, albeit under appropriate conditions. This implies that the forces that stabilize fibrils are the forces common to all proteins—hydrophobic interactions and backbone hydrogen bonding—and not the forces associated with specific interactions between side chains. It follows then that progress toward understanding the origins of various protein deposition diseases can be made by in vitro examination of the general features of protein fibrillization using model proteins that are less complex

(1) Kelly, J. W. *Curr. Opin. Struct. Biol.* **1998**, *8*, 101−106.
(2) Rochet, J. C.; Lansbury, P. T., Jr. *Curr. Opin. Struct. Biol.* **2000**, *10*, 60−68.
(3) Dobson, C. M. *Philos. Trans. R. Soc. London, Ser. B* **2001**, *356*, 133−145.
(4) Kelly, J. W. *Nat. Struct. Biol.* **2002**, *9*, 323−325.
(5) Zerovnik, E. *Eur. J. Biochem.* **2002**, *269*, 3362−3371.
(6) Sunde, M.; Blake, C. *Adv. Protein Chem.* **1997**, *50*, 123−159.
(7) Booth, D. R.; Sunde, M.; Belotti, V.; Robinson, C. V.; Hutchinson, W.; Fraser, P. E.; Hawkins, P. W.; Dobson, C. M.; Redford, S. E.; Blake, C. C. *Nature* **1997**, *385*, 787−793.
(8) Guijarro, J. I.; Sunde, M.; Jones, J. A.; Campbell, I. D.; Dobson, C. M. *Proc. Natl. Acad. Sci. U.S.A.* **1998**, *95*, 4224−4228.
(9) Chiti, F.; Webster, P.; Toddei, N.; Clark, A.; Stefan, M.; Ramponi, G.; Dobson, C. M. *Proc. Natl. Acad. Sci. U.S.A.* **1999**, *96*, 3590−3594.
(10) Blake, C.; Serpell, L. C. *Structure* **1996**, *4*, 989−998.
(11) Sunde, M.; Serpell, L. C.; Bartlam, M.; Fraser, P. E.; Pepys, M. B.; Blake, C. C. F. *J. Mol. Biol.* **1997**, *273*, 729−739.
(12) Walsh, D. M.; Lomakin, A.; Benedek, G. B.; Condron, M. M.; Teplow, D. B. *J. Biol. Chem.* **1997**, *272*, 22364−22372.
(13) Harper, J. D.; Wong, S. S.; Lieber, C. M.; Lansbury, P. T., Jr. *Chem. Biol.* **1997**, *4*, 119−125.
(14) Serpell, L. C. *Biochimica et Biophysica Acta* **2000**, *1502*, 16−30.
(15) Pallitto, M.; Murphy, R. M. *Biophys. J.* **2001**, *81*, 1805−1822.
(16) Chiti, F.; Bucciantini, M.; Capanni, C.; Taddei, N.; Dobson, C. M.; Stefan, M. *Protein Sci.* **2001**, *10*, 2541−2547.
(17) Bucciantini, M.; Giannoni, E.; Chiti, F.; Baroni, F.; Formigli, L.; Zurdo, J.; Taddei, N.; Ramponi, G.; Dobson, C. M.; Stefani, M. *Nature* **2002**, *416*, 507−511.
(18) Fezoui, Y.; Hartley, D. M.; Walsh, D. M.; Selkoe, D. J.; Osterhout, J. J.; Teplow, D. B. *Nat. Struct. Biol.* **2000**, *7*, 1095−1099.
(19) Kayed, R.; Head, E.; Thompson, J. L.; McIntire, T. M.; Milton, S. C.; Cotman, C. W.; Glabe, C. G. *Science* **2003**, *300*, 486-489.

10.1021/ja0539140 CCC: $33.50

than the specific amyloidogenic protein. Progress could also made by in silico examination of the molecular-level mechanisms responsible for the formation of fibrils by model peptides so long as the protein geometry, hydrophobicity, and hydrogen bonding are properly taken into account.

Most computer simulations of fibril-forming peptides have been devoted to the study of isolated peptides[20−28] and have employed high-resolution protein models,[29−31] which are based on a realistic representation of protein geometry and a fairly faithful accounting for the energetics of every atom on the protein and on the solvent. High-resolution simulation studies of the formation of fibrils from random coils have been conducted, but they are generally limited to early events in the assembly of a few peptides.[32−35] Although the above-mentioned studies offer considerable insight into the properties of fibrils and the mechanisms by which they are formed, the systems considered do not contain enough peptides to mimic the nucleus that stabilizes the large fibrils observed in experiments. In the past few years, however, there have been a number of attempts to simulate multipeptide systems containing already-formed amyloid fibrils.[36−43] Ma[38] conducted MD simulations using the package Discover 2.98 for up to 4 ns on a system containing an already-formed fibrillar aggregate of eight AAAAAAAA peptides that is surrounded by either a single α-helical AAAAAAAA monomer or eight random-coil AAAAAAAA peptides. They did not observe fibril growth due to the limited simulation time in either case. Given current computational capabilities, simpler models are required to simulate multiprotein systems. Computer simulations using low-resolution models, which are based on a coarse-grained representation of protein geometry and energetics, have been used by a few investigators to study protein aggregation.[44−58] Although such models provide invaluable insights into the basic physics underlying protein aggregation in general, they do not adequately account for the different forces, such as hydrogen bonding, that play an important role in fibril formation.

Intermediate-resolution protein models,[59−70] which are essentially a compromise between low-resolution models and detailed all-atom models, have been used extensively in recent years to simulate the folding of isolated proteins. They have also been used by a few investigators to study fibril formation. Jang[71,72] applied an off-lattice model with each amino acid residue represented by a single bead interacting via Go potentials[73] (which have a partial built-in bias toward the native state) to study the thermodynamics and kinetics of the assembly of four model β-sheet peptides into a tetrameric β-sheet complex. Dokholyan and co-workers applied an off-lattice model with each amino acid residue represented by one backbone bead and one side chain bead interacting via Go potentials to study the formation of fibrillar β-sheet structures by eight model Src SH3 domain proteins[74] or by 28 model Aβ(1−40) peptides.[75] These simulations provide more detail on the mechanisms that govern fibril formation than the lattice models. However, since the Go potential contains a built-in bias toward the native conformation, they are not suitable for the study of spontaneous fibril formation from random-coil configurations.

An intermediate-resolution protein model that has no built-in bias toward any conformation has been developed in our group by Smith and Hall[70,76,77] and later improved by Nguyen, Marchut and Hall.[78] Each amino acid is represented via an united atom approach—three beads for the backbone and one bead for the side chain. The model contains enough genuine protein character to mimic real protein dynamics yet is simple enough

(20) Kortvelyesi, T.; Kiss, G.; Murphy, R. F.; Penke, B.; Lovas, S. *J. Mol. Struct.* **2001**, *545*, 215−223.
(21) Straub, J. E.; Guevara, J.; Huo, S.; Lee, J. P. *Acc. Chem. Res.* **2002**, *35*, 473−481.
(22) Massi, F.; Peng, J. W.; Lee, J. P.; Straub, J. E. *Biophys. J.* **2001**, *81*, 31−44.
(23) Massi, F.; Klimov, D.; Thirumalai, D.; Straub, J. E. *Protein Sci.* **2002**, *11*, 1639−1647.
(24) Massi, F.; Straub, J. E. *J. Comput. Chem.* **2001**, *24*, 143−153.
(25) Massi, F.; Straub, J. E. *Biophys. J.* **2001**, *81*, 697−709.
(26) Moraitakis, G.; Goodfellow, J. M. *Biophys. J.* **2003**, *84*, 2149−2158.
(27) Ilangovan, U.; Ramamoorthy, A. *Biopolymers* **1998**, *45*, 9−20.
(28) Yang, M.; Lei, M.; Huo, S. *Protein Sci.* **2003**, *12*, 1222−1231.
(29) Weiner, P. K.; Kollman, P. A. *J. Comput. Chem.* **1981**, *2*, 287−303.
(30) Brooks, B. R.; Bruccoleri, R. E.; Olafson, B. D.; States, D. J.; Swaminathan, S.; Karplus, M. *J. Comput. Chem.* **1983**, *4*, 187−217.
(31) Levitt, M.; Hirschberg, M.; Sharon, R.; Daggett, V. *Comput. Phys. Commun.* **1995**, *91*, 215−231.
(32) Gsponer, J.; Haberthur, U.; Caflisch, A. *Proc. Natl. Acad. Sci. U.S.A.* **2003**, *100*, 5154−5159.
(33) Mager, P. P. *Molecular Simulation* **1998**, *20*, 201−222.
(34) Fernandez, A.; Boland, M. D. L. *FEBS Lett.* **2002**, *529*, 298−302.
(35) Klimov, D. K.; Thirumalai, D. *Structure* **2003**, *11*, 295−307.
(36) Li, L.; Darden, T. A.; Bartolotti, L.; Kominos, D.; Pedersen, L. G. *Biophys. J.* **1999**, *76*, 2871−2878.
(37) George, A. R.; Howlett, D. R. *Biopolymers* **1999**, *50*, 733−741.
(38) Ma, B.; Nussinov, R. *Protein Sci.* **2002**, *11*, 2335−2350.
(39) Ma, B.; Nussinov, R. *Proc. Natl. Acad. Sci. U.S.A.* **2002**, *99*, 14126−14131.
(40) Zanuy, D.; Ma, B.; Nussinov, R. *Biophys. J.* **2003**, *84*, 1884−1894.
(41) Zanuy, D.; Nussinov, R. *J. Mol. Biol.* **2003**, *329*, 565−584.
(42) Hwang, W.; Marini, D. M.; Kamm, R. D.; Zhang, S. *J. Chem. Phys.* **2003**, *118*, 389−397.
(43) Kuwata, K.; Matumoto, T.; Cheng, H.; Nagayama, K.; James, T. L.; Roder, H. *Proc. Natl. Acad. Sci. U.S.A.* **2003**, *100*, 4790−4795.
(44) Harrison, P. M.; Chan, H. S.; Prusiner, S. B.; Cohen, F. E. *J. Mol. Biol.* **1999**, *286*, 593−606.
(45) Leonhard, K.; Prausnitz, J. M.; Radke, C. J. *Protein Sci.* **2004**, *13*, 358−369.
(46) Patro, S. Y.; Przybycien, T. M. *Biophys. J.* **1994**, *66*, 1274−1289.
(47) Patro, S. Y.; Przybycien, T. M. *Biophys. J.* **1994**, *70*, 2888−2902.
(48) Broglia, R. A.; Tiana, G.; Pasqali, S.; Roman, H. E.; Vigezzi, E. *Proc. Natl. Acad. Sci. U.S.A.* **1998**, *95*, 12930−12933.
(49) Istrail, S.; Schwartz, R.; King, J. *J. Comput. Biol.* **1999**, *6*, 143−162.
(50) Giugliarelli, G.; Micheletti, C.; Banavar, J. R.; Maritan, A. *J. Chem. Phys.* **2000**, *113*, 5072−5077.
(51) Bratko, D.; Blanch, H. W. *J. Chem. Phys.* **2001**, *114*, 561−569.
(52) Dima, R. I.; Thirumalai, D. *Protein Sci.* **2002**, *11*, 1036−1049.
(53) Bratko, D.; Blanch, H. W. *J. Chem. Phys.* **2003**, *118*, 5185−5194.
(54) Combe, N.; Frenkel, D. *J. Chem. Phys.* **2003**, *118*, 9015−9022.
(55) Toma, L.; Toma, S. *Biomacromolecules* **2000**, *1*, 232−238.
(56) Gupta, P.; Voegler, A. C.; Hall, C. K. *Protein Sci.* **1998**, *7*, 2642−2652.
(57) Gupta, P.; Voegler, A. C.; Hall, C. K. *Fluid Phase Equilib.* **1999**, *160*, 87−93.
(58) Nguyen, H. D.; Hall, C. K. *Biotechnol. Bioeng.* **2002**, *80*, 823−834.
(59) Sikorski, A.; Kolinski, A.; Skolnick, J. *Biophys. J.* **1998**, *75*, 92−105.
(60) Sikorski, A.; Kolinski, A.; Skolnick, J. *Proteins: Struct., Funct., Genet.* **2000**, *38*, 17−28.
(61) Kolinski, A.; Skolnick, J. *J. Chem. Phys.* **1992**, *97*, 9412−9426.
(62) Kolinski, A.; Skolnick, J. *Proteins: Struct., Funct., Genet.* **1994**, *18*, 338−352.
(63) Kolinski, A.; Skolnick, J. *Proteins: Struct., Funct., Genet.* **1994**, *18*, 353−366.
(64) Sun, S. *Protein Sci.* **1993**, *2*, 762−785.
(65) Wallqvist, A.; Ullner, M. *Proteins: Struct., Funct., Genet.* **1994**, *18*, 267−280.
(66) Sun, S.; Thomas, P. D.; Dill, K. A. *Protein Eng.* **1995**, *8*, 769−778.
(67) Klimov, D. K.; Thirumalai, D. *Folding Des.* **1998**, *3*, 127−139.
(68) Li, L.; Mirny, L. A.; Shakhnovich, E. I. *Nat. Struct. Biol.* **2000**, *7*, 336−342.
(69) Takada, S.; Luthey-Schulten, Z.; Wolynes, P. G. *J. Chem. Phys.* **1999**, *110*, 11616−11629.
(70) Smith, A. V.; Hall, C. K. *Proteins: Struct., Funct., Genet.* **2001**, *44*, 344−360.
(71) Jang, H.; Hall, C. K.; Zhou, Y. *Biophys. J.* **2004**, *86*, 31−49.
(72) Jang, H.; Hall, C. K.; Zhou, Y. *Protein Sci.* **2004**, *13*, 40−53.
(73) Go, N. *Annu. Rev. Biophys. Bioeng.* **1983**, *12*, 183-210.
(74) Ding, F.; Dokholyan, N. V.; Buldyrev, S. V.; Stanley, H. E.; Shakhnovich, E. I. *J. Mol. Biol.* **2002**, *324*, 851−857.
(75) Peng, S.; Ding, F.; Urbanc, B.; Buldyrev, S. V.; Cruz, L.; Stanley, H. E.; Dokholyan, N. V. *Phys. Rev. E: Stat. Phys., Plasmas, Fluids, Relat. Interdiscip. Top.* **2004**, *69*, 041908−041914.
(76) Smith, A. V.; Hall, C. K. *Proteins: Struct., Funct., Genet.* **2001**, *44*, 376−391.
(77) Smith, A. V.; Hall, C. K. *J. Mol. Biol.* **2001**, *312*, 187−202.
(78) Nguyen, H. D.; Marchut, A. J.; Hall, C. K. *Protein Sci.* **2004**, *13*, 2909−2924.

to be computationally tractable, especially for use in computer simulations of protein aggregation in relatively large systems. This model, which we now call PRIME (*P*rotein *I*ntermediate-Resolution *M*ode*l*) is designed to be used with discontinuous molecular dynamics (DMD),[79−82] an extremely fast alternative to traditional molecular dynamics that is applicable to systems of molecules interacting via discontinuous potentials, e.g., hard-sphere and square-well potentials. The solvent is modeled implicitly by including the hydrophobic interaction between nonpolar side chains. Backbone hydrogen bonding is modeled in explicit detail. Using this DMD algorithm, we are able to sample much wider regions of conformational space, longer time scales, and larger systems than in the case of traditional molecular dynamics. As we will show in this paper, we are able to simulate the formation of fibrils from systems containing between 12 and 96 16-residue polyalanine peptides starting from the random state.

A similar approach has been taken by Ding[83] who studied the formation of amyloid beta dimers in a system containing two Aβ(1−40) or two Aβ(1−42) peptides.[84] Urbanc also examined the early stage of amyloid oligomerization in a system containing 32 Aβ(1−40) or 32 Aβ(1−42) peptides;[85] they were able to observed the formation of amorphous structures but not β-sheet or fibril structures.

The model peptide chosen for study is the polyalanine-based peptide Ac−KA_{14}K−NH_2. We focus on polyalanine-based peptides for three reasons. First, the small, uncharged, unbranched nature of alanine residues is amenable to simulation with the intermediate-resolution protein model that we developed previously.[70,76] Second, polyalanine repeats have been implicated in human pathologies, notably in the formation of anomalous filamentous intranuclear inclusions in oculopharyngeal muscular dystrophy patients.[86] Third, synthetic polyalanine-based peptides have been shown by Blondelle to undergo a transition from α-helical structures to β-sheet complexes in vitro,[87,88] mimicking the structural transition that is believed to be a prerequisite for fibril nucleation and growth.[6,44,89−93] Blondelle observed that the α-helical structures were stabilized in part by intramolecular α-helical bonds and the macromolecular β-sheet complex was stabilized by hydrophobic intersheet interactions. Using circular dichroism, Fourier transform infrared spectroscopy, and reversed-phase high performance liquid chromatography, they found that

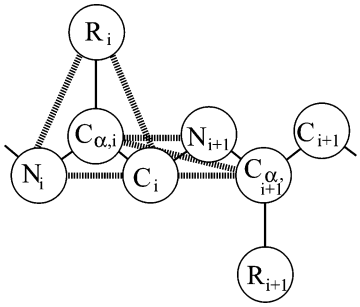

Figure 1. Covalent bonds are shown with narrow black lines connecting united atoms. At least one of each type of pseudobond is shown with a thick disjointed line. Pseudobonds are used to maintain backbone bond angles, consecutive C_α distances, and residue L-isomerization. Note that the united atoms are not shown full size for ease of viewing.

(1) β-sheet complex formation increased with increasing temperature, exhibiting an S-shaped dependence on temperature with a critical temperature of 45 °C at a peptide concentration of 1.8 mM and an incubation time of 3 h, and (2) β-sheet complex formation increased with increasing peptide concentration above a critical concentration of 1 mM at 65 °C.

In this paper, we investigate how peptide concentration and temperature affect the formation of various Ac−KA_{14}K−NH_2 structures including α-helices, β-sheets, and fibrils. Simulations are conducted on systems of 12, 24, 48, and 96 model 16-residue peptides at a wide variety of concentrations and temperatures by applying the discontinuous molecular dynamics simulation algorithm to our intermediate-resolution protein model. All simulations are performed in the canonical ensemble starting from a random coil configuration equilibrated at a high temperature and then slowly cooled to the temperature of interest so as to minimize kinetic trapping in local free energy minima. The percentage of peptides that form α-helices, β-sheets, or fibrils is monitored during the simulation. In addition, structural characteristics such as the peptide arrangement and packing of fibrils are examined and compared with those observed in experiments. We also study the overall stability of fibrils by conducting simulations on already-formed fibrils over a wide range of temperatures to investigate the relative importance of hydrogen bonding and hydrophobic interactions on fibril stability. The stability of our fibrillar structures is evaluated by comparing the abilities of the system to maintain the fibrillar structures at various temperatures which are higher than the fibril formation temperature.

Models and Methods

Model Peptide and Forces. The model peptide has the sequence $PH_{14}P$, where H is a hydrophobic amino acid residue and P is a polar amino acid residue. This sequence was chosen to mimic Ac−KA_{14}K−NH_2 peptides which have been shown to form stable, soluble β-sheet complexes.[87,88] The peptide is modeled using PRIME, an intermediate-resolution model[70,76,77] based on a united-atom approach with realistic bond lengths and bond-angle constraints that has the ability to interact both intra- and intermolecularly via hydrogen bonding and hydrophobic interaction potentials. The geometry of the protein model is illustrated in Figure 1. Each amino acid residue is composed of four spheres, a three-sphere backbone comprised of united atom NH, C_αH, and C═O, and a single-bead side chain R (labeled N, C_α, C, and R, respectively in the figure). All backbone bond lengths and bond angles are fixed at their ideal values; the distance between consecutive C_α atoms is fixed so as to maintain the interpeptide bond in the trans configuration. The side chains are held in positions relative to the backbone so that all

(79) Alder, B. J.; Wainwright, T. E. *J. Chem. Phys.* **1959**, *31*, 459−466.
(80) Rapaport, D. C. *J. Phys. A: Math. Gen.* **1978**, *11*, L213-L217.
(81) Rapaport, D. C. *J. Chem. Phys.* **1979**, *71*, 3299−3303.
(82) Bellemans, A.; Orban, J.; VanBelle, D. *Mol. Phys.* **1980**, *39*, 781−782.
(83) Ding, F.; Borreguero, J. M.; Buldyrey, S. V.; Stanley, H. E.; Dokholyan, N. V. *Proteins: Struct., Funct., Genet.* **2003**, *53*, 220−228.
(84) Urbanc, B.; Cruz, L.; Ding, F.; Sammond, D.; Khare, S.; Buldyrey, S. V.; Stanley, H. E.; Dokholyan, N. V. *Biophys. J.* **2004**, *87*, 2310−2321.
(85) Urbanc, B.; Cruz, L.; Yun, S.; Buldyrey, S. V.; Bitan, G.; Teplow, D. B.; Stanley, H. E. *Proc. Natl. Acad. Sci. U.S.A.* **2004**, *101*, 17345−17350.
(86) Brais, B.; Rouleau, G. A.; Bouchard, J. P.; Farde, M.; Tome, F. M. S. *Seminars in Neurology* **1999**, *19*, 59−66.
(87) Forood, B.; Perez-Paya, E.; Houghten, R. A.; Blondelle, S. E. *Biochem. Biophys. Res. Commun.* **1995**, *211*, 7−13.
(88) Blondelle, S. E.; Forood, B.; Houghten, R. A.; Perez-Paya, E. *Biochemistry* **1997**, *36*, 8393−8400.
(89) Kirschner, D. A.; Abraham, C.; Selkoe, D. J. *Proc. Natl. Acad. Sci. U.S.A.* **1986**, *83*, 503−507.
(90) Simmons, L.; May, P.; Tomaselli, K.; Rydel, R.; Fuson, K.; Brigham, E.; Wright, S.; Lieberburg, I.; Becker, G.; Brems, D.; Li, W. *Mol. Pharmacol.* **1994**, *45*, 373−379.
(91) Horwich, A. L.; Weissman, J. S. *Cell* **1997**, *89*, 499−510.
(92) Kusumoto, Y.; Lomakin, A.; Teplow, D. B.; Benedek, G. B. *Proc. Natl. Acad. Sci. U.S.A.* **1998**, *95*, 12277−12282.
(93) Esler, W. P.; Felix, A. M.; Stimson, E. R.; Lachenmann, M. J.; Ghilardi, J. R.; Lu, Y. A.; Vinters, H. V.; Mantyh, P. W.; Lee, J. P.; Maggio, J. E. *J. Struct. Biol.* **2000**, *130*, 174−183.

residues are L-isomers. Details of the model including values for all parameters are given in our earlier papers.[70,78]

The solvent is modeled implicitly in the sense that its effect is factored into the energy function as a potential of mean forces. All forces are modeled by either a hard-sphere potential,

$$u_{ij}(r) = \begin{cases} \infty, r \le \sigma \\ 0, r > \sigma \end{cases} \quad (1)$$

where r is the distance between spheres i and j and σ is the sphere diameter, or a square-well potential

$$u_{ij}(r) = \begin{cases} \infty, r \le \sigma \\ -\epsilon, \sigma < r \le \lambda\sigma \\ 0, r > \lambda\sigma \end{cases} \quad (2)$$

where $\lambda\sigma$ is the well diameter and ϵ is the well depth. The excluded volumes of the four united atoms are modeled using hard-sphere potentials with realistic diameters. Covalent bonds are maintained between adjacent spheres along the backbone by imposing hard sphere repulsions whenever the bond lengths attempt to move outside of the range between $l(1 - \delta)$ and $l(1 + \delta)$ where l is the bond length and δ is a tolerance which we set equal to 2.375%. Ideal backbone bond angles, $C_\alpha - C_\alpha$ distances, and residue L-isomerization are achieved by imposing pseudobonds, as shown in Figure 1, which also fluctuate within a tolerance of 2.375%. Interactions between hydrophobic side chains are represented by a square-well potential of depth ϵ_{HP} and range 1.5 σ_R, where σ_R is the side chain diameter. Hydrophobic side chains must be separated by at least three intervening residues in order to interact. Hydrogen bonding between amide hydrogen atoms and carbonyl oxygen atoms on the same or neighboring chains is represented by a square-well attraction between NH and C=O united atoms. For more details on the hydrogen bonding model used here, see a recent paper by Nguyen, Marchut, and Hall.[78] For simplicity, the strength of a hydrophobic contact, ϵ_{HP}, is fixed at 1/10, 1/8, and 1/6 the strength of a hydrogen bond, ϵ_{HB}. Hydrogen bond strength and hydrophobic contact strength are independent of temperature, as has been assumed in previous simulation studies.[76,77,94,95]

Discontinuous Molecular Dynamics. Simulations are performed using the discontinuous molecular dynamics (DMD) simulation algorithm,[79−82] which is an extremely fast alternative to traditional molecular dynamics and is applicable to systems of molecules interacting via discontinuous potentials, e.g., hard-sphere and square-well potentials. For more details on DMD simulations with square-well potentials, see papers by Alder and Wainwright[79] and Smith, Hall, and Freeman.[96] All simulations are performed at constant temperature which is achieved by implementing the Andersen thermostat method[97] as was used previously.[70,98] With this procedure, all united atoms in the simulation are subject to random collisions with ghost particles. The postevent velocity of an united atom colliding with a ghost particle is chosen randomly from a Maxwell−Boltzmann distribution at the simulation temperature.

For the fibril formation simulations, each system was started from a random-coil configuration equilibrated at a high temperature, $T^* = 0.16$, and then cooled to the temperature of interest ($T^* = 0.08$, 0.09, 0.10, 0.11, 0.12, 0.13, 0.14, and 0.15) to minimize kinetic trapping in local free energy minima. The cooling rate is set by varying the number of ghost particles; the more ghost particles there are, the quicker the system reaches the temperature of interest. An initial test run at different cooling rates demonstrates that if the system is quickly quenched to a low temperature, all peptides rapidly assemble into an amorphous aggregate whose energy is higher than that of the fibril obtained by cooling the system down slowly. Since we are interested in observing fibrils obtained at equilibrium, all systems were cooled slowly; the number of ghost collisions was set at 0.005% of the total number of collisions during a simulation. The resulting cooling rate is $\Delta T^*/\Delta t^* = 0.0004$, where t^* is the reduced time which is defined as $t/\sigma\sqrt{k_B T/m}$ with t as the simulation time, and σ and m as the average united atom diameter and mass. For these simulations, we use cubic boxes with sides ranging from 158 to 542 Å in length depending on the peptide concentration.

Although simulations were conducted on systems containing 12, 24, 48, and 96 peptides, we focus most of our analysis on the 48-peptide system. The peptide packing fraction NV_p/V for the 48-peptide system ranges from 0.001 26 to 0.050 67 where $N = 48$ is the number of peptides, V is the total system volume, and the peptide volume $V_p \equiv 4\pi R_g^3/3$ ($R_g = 9.98$ Å is the average peptide radius of gyration in our simulations when the peptide is in the random-coil conformation). The peptide concentrations for the 48-peptide system are $c \equiv N/N_A V \approx$ 0.5, 1, 2.5, 5, 10, and 20 mM where N_A is Avogadro's number. Though our system is small compared with real fibrils (actually protofilaments) which tend to contain four to six β-sheets with 1000 or more peptides per sheet,[11,99−101] it is quite large compared with the few peptides simulated in other studies.[32−34,102,103] Hopefully this is sufficient to provide a foundation for the basic understanding of fibril formation in larger systems. Simulations were performed for between 8E9 and 32E9 events, which required 40 h at $T^* = 0.08$ for 8E9 events to 160 h at $T^* = 0.15$ for 32E9 events on a single processor of an AMD Athlon MP 2200+ workstation for the 48-peptide system. All systems were simulated for long periods of time until the ensemble averages of the system's total potential energy varied by no more than 2.5% during the last three-quarters of each simulation run. Our results are reported in terms of the average percentage of peptides in the system that form the structures of interest, which were defined previously.[104]

For the fibril stability simulations, each system was started from a 48-peptide fibrillar structure, which was formed at $c = 5$ mM and $T^* = 0.11$ by the slow-cooling method described above, and then quickly heated to the temperature of interest. The number of ghost collisions was set at 0.05% of the total number of collisions during a simulation, which is sufficient to maintain the system temperature at a constant desired value. These simulations were performed at seven different reduced temperatures $T^* = 0.12$, 0.13, 0.14, 0.15, 0.16, 0.17, and 0.18, each for 10E9 events, which required 50 h on a single processor of an AMD Athlon MP 2200+ workstation.

The criteria for defining different structures such as α-helix, β-sheets, fibrils, and amorphous aggregates are given in a previous publication.[105]

Results and Discussion

Since this paper builds upon previous work by Nguyen, Marchut, and Hall[78] on the folding thermodynamics of a single peptide of the same sequence, it is useful to briefly review those results that are pertinent to the discussion here. The peptide's thermodynamics was explored using the replica exchange simulation method to map out the conformational transitions

(94) Irback, A.; Sjunnesson, F.; Wallin, S. *Proc. Natl. Acad. Sci. U.S.A.* **2000**, *97*, 13614−13618.
(95) Knott, M.; Chan, H. S. *Chem. Phys.* **2004**, *307*, 187−199.
(96) Smith, S. W.; Hall, C. K.; Freeman, B. D. *J. Comput. Phys.* **1997**, *134*, 16−30.
(97) Andersen, H. C. *J. Chem. Phys.* **1980**, *72*, 2384−2393.
(98) Zhou, Y.; Karplus, M.; Wichert, J. M.; Hall, C. K. *J. Chem. Phys.* **1997**, *107*, 10691−10708.
(99) Malinchik, S. B.; Inouye, H.; Szumowski, K. E.; Kirschner, D. A. *Biophys. J.* **1998**, *74*, 537−545.
(100) Burkoth, T. S.; Benzinger, T. L. S.; Urban, V.; Morgan, D. M.; Gregory, D. M.; Thiyagarajan, P.; Botto, R. E.; Meredith, S. C.; Lynn, D. G. *J. Am. Chem. Soc.* **2000**, *122*, 7883−7889.
(101) Serpell, L. C.; Sunde, M.; Benson, M. D.; Tennent, G. A.; Pepys, M. B.; Fraser, P. E. *J. Mol. Biol.* **2000**, *300*, 1033−1039.
(102) Mager, P. P. *Med. Res. Rev.* **1998**, *18*, 403−430.
(103) Mager, P. P.; Reinhardt, R.; Fischer, K. *Molecular Simulation* **2001**, *26*, 367−379.
(104) Nguyen, H. D.; Hall, C. K. *Biophys. J.* **2004**, *87*, 4122−4134.
(105) Nguyen, H. D.; Hall, C. K. *J. Biol. Chem.* **2005**, *280*, 9074−9082.

among the random coil, α-helix, and β-structure at different temperatures. The effect of solvent conditions on the peptide's stability was also investigated by varying the ratio R of the strength of the hydrophobic interaction (ϵ_{HP}) to that of the hydrogen bond (ϵ_{HB}), $R \equiv \epsilon_{HP}/\epsilon_{HB}$. At each hydrophobic interaction strength, we calculated the conformational free energy of each structural state to determine the structure with the lowest free energy at each temperature and identify the conformational transition between different structural states at different temperatures. We found that peptides in our simulations tend to mimic real polyalanines in that they can exist in three distinct structural states: α-helices, β-structures, and random coils, depending upon the solvent conditions. At low values of the hydrophobic interaction strength between nonpolar side chains, i.e., $R = 0$, 1/12, and 1/10, the polyalanines undergo a relatively sharp transition between an α-helical conformation at low temperatures and a random-coil conformation at high temperatures. Increasing the hydrophobic interaction strength to $R =$ 1/8, 1/6, and 1/4 induces a second transition to a β-structure, resulting in an α-helical conformation at low temperatures, a β-structure at intermediate temperatures, and a random-coil at high temperatures. At very high values of the hydrophobic interaction strength, i.e., $R \geq 1/2$, polyalanines become β-structures at low temperatures and random coils at high temperatures. At low and intermediate values of hydrophobic interaction strength, i.e., $R < 1/2$, the transition temperatures between an α-helical state to a non-α-helical state are between $T^* = 0.085$ and $T^* = 0.11$. These results are qualitatively in good agreement with experiments which show that polyalanine adopts an α-helical conformation in hydrophobic environments such as the solid state or in nonpolar organic solutions and a β-structure conformation in polar aqueous solution.[88,106−111] This is similarly observed in experiments on many heterogeneous peptides which can be folded into alternative stable structures by changing the solution conditions such as the pH, salt, or organic cosolvent concentration, peptide concentration, and the redox state.[112−126]

Interestingly, Knott and Chan[95] recently investigated the impact of the relative strengths of the hydrophobic and hydrogen bonding interaction on folding of polypeptide chains using a similar intermediate-resolution protein model[94] but with a continuous potential. When the hydrophobic interaction strength was relatively weak, they observed that the peptides exhibit certain cooperative features of the transition between native (helical) and denatured states. When the hydrophobic interaction strength was too strong, the peptides collapsed into compact conformations with little helical content. We also compared our simulation results when $R = 0$ with the Zimm−Bragg theory.[127] We found that our propagation parameter was in good agreement with experimental results that yield estimates for alanine between 1.33 and 2.19. However, our nucleation parameter (∼0.03) was much larger than the experimental estimates (∼0.003−0.004).

We then investigated the kinetics of fibril formation of Ac−$KA_{14}K$−NH_2 peptides as a function of the peptide concentration and temperature.[105,128] Constant-temperature simulations were conducted on systems containing 48 model 16-residue peptides in the canonical ensemble at a wide variety of concentrations and temperatures. During each simulation, the formation of different structures such as α-helices, amorphous aggregates, β-sheets, or fibrils was monitored as a function of time. Key fibril-forming events were identified and compared with proposed fibril-formation mechanisms appearing in the literature. The lag time before fibril formation commences decreased with increasing concentration and increased with increasing temperature. In addition, fibril formation appeared to undergo a process in which small amorphous aggregates → β-sheets → ordered nucleus → subsequent rapid growth of a stable fibril. Fibril growth in our simulations involved both β-sheet elongation, in which the fibril grows by adding individual peptides to the end of each β-sheet, and lateral addition, in which the fibril grows by adding already-formed β-sheets to its side. Once the fibrils attained a size of six sheets, they grew further through a β-sheet elongation mechanism. Moreover, the rate of fibril formation increased with increasing concentration and decreased with increasing temperature.

We also performed replica exchange equilibrium simulations on systems containing 96 Ac−$KA_{14}K$−NH_2 over a very wide range of temperatures and peptide concentrations to study the system's thermodynamics.[104] The goal here was to map out a phase diagram in the temperature−concentration plane delineating the regions where random coils, α-helices, β-sheets, fibrils, and amorphous aggregates are stable. Based on the system heat capacity and peptide radius of gyration, and on data on the percentage of the peptides that form the various structures, a phase diagram in the temperature−concentration plane was constructed. We found four distinctive single-phase regions (α-helices, fibrils, nonfibrillar β-sheets, and random coils) and four two-phase regions (random coils/nonfibrillar β-sheets, random coils/fibrils, fibrils/nonfibrillar β-sheets, and α-helices/nonfibrillar β-sheets). The α-helical region is at low temperature and low concentration. The nonfibrillar β-sheet region is at intermediate temperatures and expands to higher temperatures as concentration is increased. The fibril region is primarily at

(106) Ingwall, R. T.; Scheraga, H. A.; Lotan, N.; Berger, A.; Katchalski, E. *Biopolymers* **1968**, *6*, 331−368.
(107) Platzer, K. E. B.; Ananthanarayanan, V. S.; Andreatta, R. H.; Scheraga, H. A. *Macromolecules* **1972**, *5*, 177−187.
(108) Shoji, A.; Ozaki, T.; Fujito, T.; Deguchi, K.; Ando, S.; Ando, I. *J. Am. Chem. Soc.* **1990**, *112*, 4693−4697.
(109) Kimura, H.; Ozaki, T.; Sugisawa, H.; Deguchi, K.; Shoji, A. *Macromolecules* **1998**, *31*, 7398−7403.
(110) Lee, D. K.; Ramamoorthy, A. *J. Phys. Chem. B* **1999**, *103*, 271−275.
(111) Warrass, R.; Wieruszeski, J. M.; Boutillon, C.; Lippens, G. *J. Am. Chem. Soc.* **2000**, *122*, 1789−1795.
(112) Rosenheck, K.; Doty, P. *Proc. Natl. Acad. Sci. U.S.A.* **1961**, *47*, 1775−1785.
(113) Kabsch, W.; Sander, S. *Proc. Natl. Acad. Sci. U.S.A.* **1984**, *81*, 1075−1078.
(114) Mutter, M.; Hersperger, R. *Angew. Chem., Int. Ed. Engl.* **1990**, *29*, 185−187.
(115) Mutter, M.; Gassmann, R.; Buttkus, U.; Altmann, K. H. *Angew. Chem., Int. Ed. Engl.* **1991**, *30*, 1514−1516.
(116) Reed, J.; Kinzel, V. *Biochemistry* **1991**, *30*, 4521−4528.
(117) Zhong, L.; Johnson, W. C. *Proc. Natl. Acad. Sci. U.S.A.* **1992**, *89*, 4462−4465.
(118) Cohen, B. I.; Presnell, S. R.; Cohen, F. E. *Protein Sci.* **1993**, *2*, 2134−2145.
(119) Dado, G. P.; Gellman, S. H. *J. Am. Chem. Soc.* **1993**, *115*, 12609−12610.
(120) Waterhous, D. V.; Johnson, W. C. *Biochemistry* **1994**, *33*, 2121−2128.
(121) Cerpa, R.; Cohen, F. E.; Kuntz, I. D. *Folding & Design* **1996**, *1*, 91−101.
(122) Schenck, H. L.; Dado, G. P.; Gellman, S. H. *J. Am. Chem. Soc.* **1996**, *118*, 12487−12494.
(123) Fukushima, Y. *Bull. Chem. Soc. Jpn.* **1996**, *69*, 701−708.
(124) Zhang, S.; Rich, A. *Proc. Natl. Acad. Sci. U.S.A.* **1997**, *94*, 23−28.
(125) Tuchscherer, G.; Grell, D.; Mathieu, M.; Mutter, M. *J. Pept. Res.* **1999**, *54*, 185−194.
(126) Awasthi, S. K.; Shankaramma, S. C.; Raghothama, S.; Balaram, P. *Biopolymers* **2001**, *58*, 465−476.
(127) Zimm, B. H.; Bragg, J. K. *J. Chem. Phys.* **1959**, *31*, 526−535.
(128) Nguyen, H. D.; Hall, C. K. *Proc. Natl. Acad. Sci. U.S.A.* **2004**, *101*, 16180−16185.

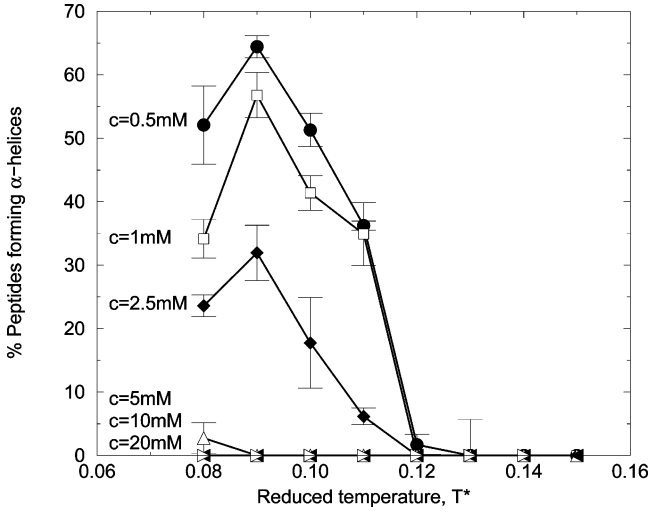

Figure 2. Percentage of peptides in the α-helical conformation obtained at the end of simulations at different temperatures and concentrations.

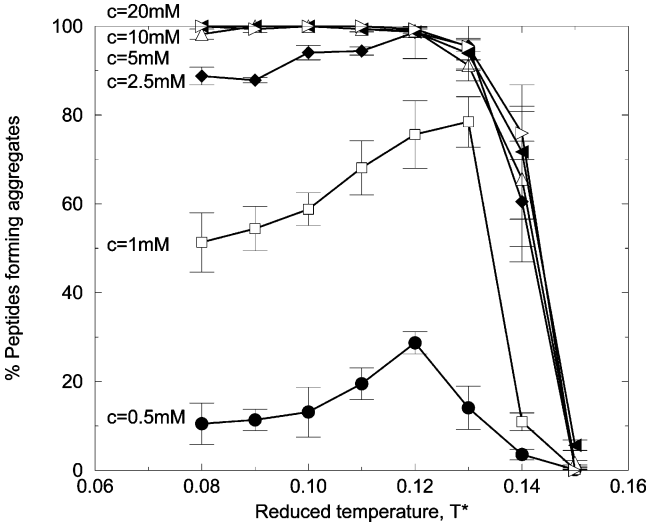

Figure 3. Percentage of peptides in aggregates obtained at the end of simulations at different temperatures and concentrations.

intermediate temperatures and intermediate concentrations and expands to lower temperatures as the peptide concentration is increased. The random-coil region is at high temperatures and all concentrations and shifts to higher temperatures as the concentration is increased.

Fibril Formation as a Function of Temperature and Concentration. In this section, we present the results from our fibril formation simulations of 48-peptide systems initially in a random-coil configuration. Simulations are conducted at concentrations $c = 0.5$, 1, 2.5, 5, 10, and 20 mM, which range from the very dilute regime, in which most peptides do not interact with neighboring peptides, to the highly concentrated regime, in which most peptides are in contact with neighboring peptides. At each concentration, simulations are performed at temperatures $T^* = 0.08$, 0.09, 0.10, 0.11, 0.12, 0.13, 0.14, and 0.15, which ranges from temperatures that are well below the folding temperature for a single α-helix ($T^* = 0.11$) to a temperature ($T^* = 0.15$) that is so high that the peptides cannot form or maintain hydrogen bonds or hydrophobic interactions, and are in random-coil conformations. The parameter $R \equiv \epsilon_{HP}/\epsilon_{HB}$ is set at 1/10. The results at each concentration and temperature are taken from the end of at least three different runs. If the potential energy of the system from three initial runs varied by more than 2.5%, then up to three more runs were conducted as warranted.

The percentage of peptides in each structure of interest is highly dependent on environmental conditions such as the temperature and the peptide concentration. In terms of forming α-helices, it is evident from Figure 2, which plots the percentage of peptides that form α-helices versus temperature at different concentrations, that there is an inverse relationship between the percentage of peptides that form this structure and the concentration. α-Helices are unlikely to be formed at concentrations greater than or equal to 5 mM. There is an optimal range of temperatures for forming α-helices; at concentrations that are less than 5 mM, the temperature at which formation of α-helices is at a maximum is $T^* = 0.09$. The maximum percentage of peptides observed to form α-helices in this study is about 65% and occurs at $T^* = 0.09$ and $c = 0.5$ mM. At low temperatures ($T^* < 0.09$) and low concentrations ($c < 5$ mM), the system is kinetically trapped; in this case, the system forms either isolated β-structures (data not shown) or aggregates that are mostly amorphous (discussed below) instead of α-helices. At temperatures higher than 0.09 and low concentrations ($c < 5$ mM), the percentage of peptides that form α-helices decreases as the temperature increases, ending at a minimum of zero percent at $T^* = 0.12$. As the concentration decreases from $c = 2.5$ mM to 1.0 mM and then 0.5 mM, the midpoint between the maximum and the minimum percentages of peptides that form α-helices at each concentration gets close to $T^* = 0.11$, the midpoint of the folding transition (50% helicity) of a single peptide from our previous simulations.[78] As the system gets diluted below $c = 0.5$ mM, these two transition midpoints are expected to converge.

Aggregation is relatively high for all concentrations except $c = 0.5$ mM over a relatively wide range of temperatures spanning from $T^* = 0.08$ to 0.14 as shown by Figure 3, which plots the percentage of peptides in (all types of) aggregates as a function of temperature at various concentrations. At high concentrations, $c = 5-20$ mM, 100% of the peptides in the system form aggregates. As the concentration decreases to $c = 2.5$ mM, the aggregation percentage decreases slightly at intermediate temperatures ($T^* = 0.10-0.11$) and somewhat more significantly at low temperatures ($T^* = 0.08-0.09$). As the concentration decreases further to $c = 1$ mM, the aggregation percentage decreases to 50% at low temperatures ($T^* = 0.08$) and 75% at high temperatures ($T^* = 0.13$). As the concentration decreases to $c = 0.5$ mM, the aggregation percentage decreases significantly to 10% at low temperatures ($T^* = 0.08$) and 30% at high temperatures ($T^* = 0.12$).

There is a conformational transition from α-helices at low temperatures to β-sheets at high temperatures for systems at intermediate concentrations ($c = 1-2.5$ mM) as can be seen by comparing the results in Figure 2 and Figure 4, which depicts the percentage of peptides in β-sheets as a function of temperature at different concentrations. For example, at $c = 1$ mM, when $T^* = 0.09$, 55% of the peptides are α-helical and 5% of the peptides are in β-sheets, but at $T^* = 0.13$, none of the peptides are α-helical and 75% of the peptides are in β-sheets. The transition from α-helical structures to β-sheet complexes, which is similarly observed in vitro by Blondelle for polyalanine peptides,[87,88] mimics the structural transition believed to be a

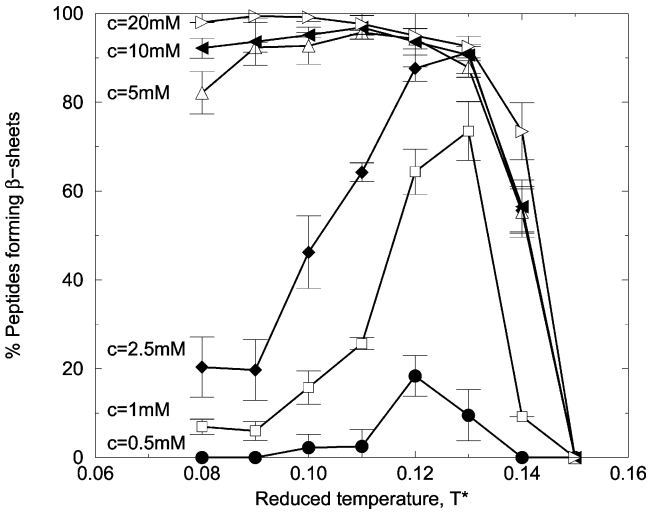

Figure 4. Percentage of peptides in β-sheet structures obtained at the end of simulations at different temperatures and concentrations.

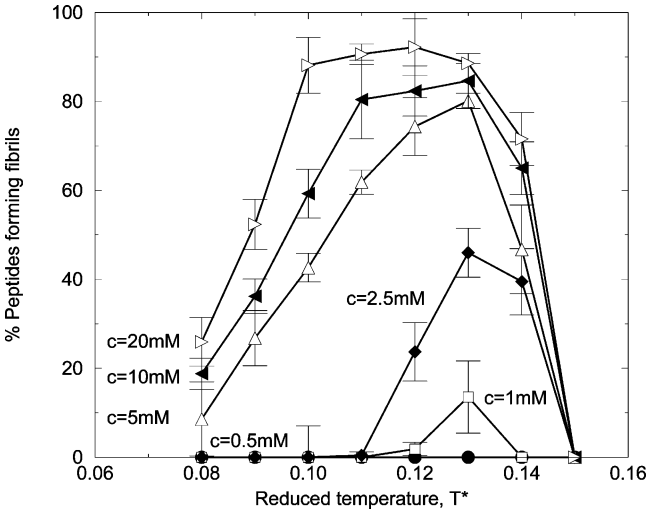

Figure 5. Percentage of peptides in fibrillar structures obtained at the end of simulations at different temperatures and concentrations.

prerequisite for fibril nucleation and growth in general.[6,44,89−93] At low concentrations ($c = 0.5$ mM), the system forms relatively few β-sheet peptides; in fact, the maximum percentage of peptides that form β-sheets at these low concentrations is only about 20% at high temperatures ($T^* = 0.12$). At high concentrations ($c = 5-20$ mM), the system forms a very high number of β-sheet peptides over a relatively large range of temperatures. When comparing the results in Figures 3 and 4 for systems at $c = 5-10$ mM, it is evident that most aggregated peptides are in β-sheets.

Fibril formation is seen only at high temperatures and high concentrations as indicated in Figure 5, which depicts the percentage of peptides in fibrils as a function of temperature at different concentrations. At high concentrations, $c = 5$, 10, and 20 mM, the dependency of fibril formation on the temperature is similar; fibril formation increases as the temperature increases up to $T^* = 0.13$ then decreases as the temperature increases further. However, as the concentration is increased from $c = 5$ mM to $c = 20$ mM, the maximum in the percentage of peptides in fibrils broadens to include lower temperatures. For example, the temperature range for the $c = 5$ mM system within which fibril formation is high is between $T^* = 0.13$ and $T^* = 0.12$.

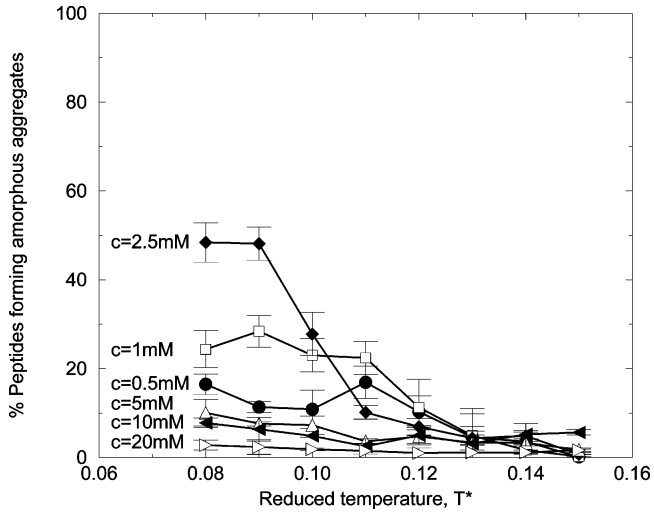

Figure 6. Percentage of peptides in amorphous structures obtained at the end of simulations at different temperatures and concentrations.

The lower limit of this range moves to $T^* = 0.11$ for the $c = 10$ mM system and then to $T^* = 0.10$ for the $c = 20$ mM system. In other words, the critical temperature for forming fibrils decreases with peptide concentration, which is similarly observed in vitro by Blondelle for polyalanine peptides.[88] The maximum percentage of peptides observed to form fibrils in this study is about 90% and occurs at $T^* = 0.10-0.13$ for the $c = 20$ mM system. A comparison of Figures 4 and 5 shows that only a portion of the β-sheet peptides form fibrils. At low temperatures ($T^* = 0.08-0.09$) and high concentrations ($c = 5-10$ mM), the β-sheets tend to stick together at a relatively large angle (i.e., greater 35°) resulting in a low yield of fibrils. At high temperatures ($T^* = 0.13-0.14$) and intermediate concentrations ($c = 1-2.5$ mM), the β-sheets tend to be isolated without forming fibrils.

The formation of amorphous aggregates is seen mostly at intermediate concentrations ($c = 1-2.5$ mM) and low temperatures ($T^* = 0.08-0.09$) as shown in Figure 6, which plots the percentage of peptides in amorphous aggregates as a function of temperature at various concentrations. This figure indicates that the highest percentage of the peptides that form amorphous aggregates is around 50% at $c = 2.5$ mM. The aggregates formed at this condition contain α-helices as can be seen by comparing the results in Figures 2 and 3 for systems at $c = 1.0$, and 2.5 mM and at $T^* = 0.08-0.09$. For example, at $c = 2.5$ mM about 30% of the peptides in the system form either isolated or attached α-helices, while 90% of the peptides form aggregates; at least 20% of the peptides that are α-helices reside inside aggregates (data not shown). The α-helices that reside inside of aggregates are more stable than isolated α-helices, since each aggregated α-helix can form multiple extra hydrophobic interactions with neighboring peptides. The systems that form amorphous aggregates at intermediate concentrations and low temperatures are believed to be kinetically trapped in local minima. Unlike low concentrations where peptides form isolated α-helices, and high concentrations where peptides form β-sheets, at intermediate concentrations any isolated α-helices that are formed immediately cluster together resulting in an amorphous structure. Although the peptides may try to unfold to form ordered aggregates, they remain trapped because of the low temperature.

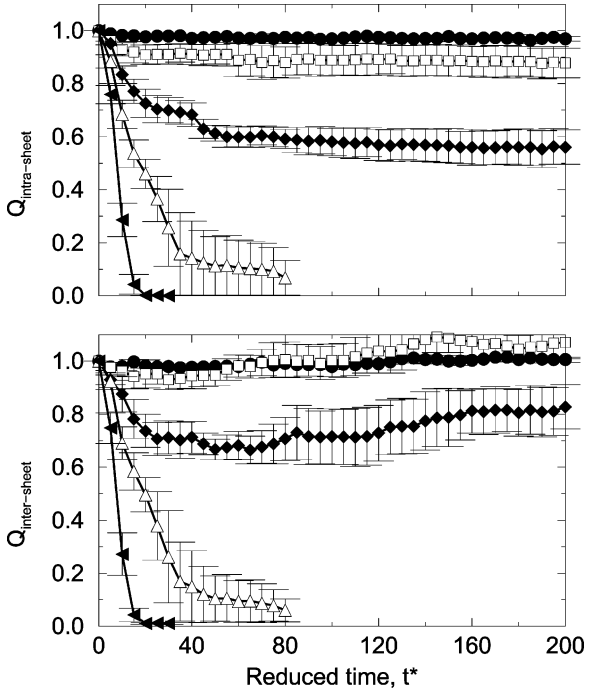

Figure 7. Fibril stability parameters $Q_{intrasheet}$ and $Q_{intersheet}$ versus reduced time, t^*, from simulations starting with fibrils formed at $T^* = 0.11$ performed at $T^* = 0.14$ (●), $T^* = 0.15$ (□), $T^* = 0.16$ (◆), $T^* = 0.17$ (△), and $T^* = 0.18$ (▲).

Fibril Stability. In our fibril stability simulations, fibrils are stable at temperatures above those at which the α-helical model peptides are stable as indicated in Figure 7, which is a plot of the fibril order parameters, $Q_{intrasheet}$ and $Q_{intersheet}$, as a function of time during the high-temperature stability simulations at $T^* = 0.14$, 0.15, 0.16, 0.17, and 0.18. The quantity $Q_{intrasheet}$ is defined as the sum of the numbers of intrasheet hydrogen bonds and intrasheet hydrophobic interactions within those β-sheets present in the original fibril that are still present at time t^* divided by the sum of their initial numbers. In other words, $Q_{intrasheet} - 1$ measures the number of hydrogen bonds and hydrophobic interactions broken and formed on the peptides within each original β-sheet, and hence $Q_{intrasheet}$ represents the intrasheet stability. The quantity $Q_{intersheet}$ is defined as the number of intersheet hydrophobic interactions between β-sheets present in the original fibril that are still present at time t^* divided by their initial number; $Q_{intersheet} - 1$ measures the number of intersheet hydrophobic interactions broken and formed, and hence $Q_{intersheet}$ represents the intersheet stability. In each simulation, the starting configuration is the structure formed at the end of a simulation at $T^* = 0.11$ which itself started out as a system of random coils. The system is instantaneously heated to the temperature of interest, and thereafter the temperature remains constant. The order parameters for the initial structures are unity ($Q_{intrasheet}$ and $Q_{intersheet} = 1$). At the lowest temperatures in the range $T^* = 0.12-0.13$, the fibril system stays in the original structure for extended times (data not shown). As seen in Figure 7, the fibril continues to maintain its stability over extended times at $T^* = 0.14$.

The fibril can recover its original stability along the fibril axis more easily than perpendicular to the fibril axis when exposed to high temperatures as indicated by the values of the order parameters $Q_{intrasheet}$ and $Q_{intersheet}$ at $T^* = 0.15$ (Figure 7). In this case, the fibril gradually loses a small amount of its original intrasheet stability over long periods of time; on the other hand, the fibril loses a small amount of its original intersheet stability only at the beginning of the simulations but then regains and even strengthens its intersheet stability toward the end of the simulations. The fibril gains this additional intersheet stability by shifting each β-sheet a small distance so as to maximize the number of intersheet hydrophobic contacts. At a slightly higher temperature, $T^* = 0.16$, the fibril loses approximately 45% of its original intrasheet contacts at long times. Although the fibril initially loses approximately 30% of its original intersheet contacts, it regains some of its intersheet stability; after long times, it has lost only 20% of its original intersheet contacts. At $T^* = 0.17-0.18$, the fibril quickly loses most of its original contacts and disperses into random coils.

Our fibrillar complexes are stable at higher temperatures than the isolated α-helices are stable, which is similar to experimental results on polyalanine-based peptides.[87,110] The temperature at which the fibril starts to lose a significant fraction of its original contacts in our simulations as indicated in Figure 7 is $T^* = 0.16$, which is well above the unfolding temperature for isolated α-helices ($T^* = 0.11$) from a previous study.[78] In our systems, the model fibrils are more stable than the model isolated α-helices at high temperatures because model fibrils contain more hydrogen bonds. Each peptide within a β-sheet of a fibril can form up to 15 interpeptide hydrogen bonds to each of its two neighboring peptides and zero intrapeptide hydrogen bonds. This can be compared to just 12 intrapeptide hydrogen bonds and zero interpeptide hydrogen bonds formed by an isolated α-helix. Moreover, inter-peptide hydrophobic contacts, which are numerous in systems of model fibrils, are not present in diluted systems of model α-helices which rarely interact with each other.

Fibril growth takes place at higher temperatures than fibril formation as indicated in Figure 8, which plots the average number of peptides per β-sheet per fibril and the average number of β-sheets per fibril over time t^* from fibril stability simulations at $T^* = 0.15$ and $T^* = 0.16$. Compared with Figure 5, which shows that fibril formation happens only at temperatures that are up to $T^* = 0.14$, the already-formed fibril in Figure 8 continues to grow at $T^* = 0.15$ by adding monomeric peptides that are still available in the system to the ends of the β-sheets. This suggests that fibril formation requires the presence of a nucleus. Such nucleation will be explored in more detail in a future publication.

The fibril is more stable along the fibril axis than perpendicular to it at high temperatures as indicated in Figure 8 for $T^* = 0.16$. When instantaneously exposed to high temperature, the fibril quickly loses more than 30% of its original number of β-sheets, which then disintegrate into monomeric peptides (data not shown). On the other hand, peptides in the remaining β-sheets not only maintain their numbers but also continue to grow slightly.

Fibril Structure. The fibrils observed in our simulations mimic the structural characteristics of fibrillar aggregates currently described in the literature. Specifically, most peptides within each β-sheet of our fibrils are arranged in a parallel orientation. In fact, the percentage of peptides whose C-terminus are on a particular side of their β-sheet in the fibril (with N-terminus on the other side) compared with the total number of peptides in that β-sheet in the fibril is 93.3% (±5.7) for

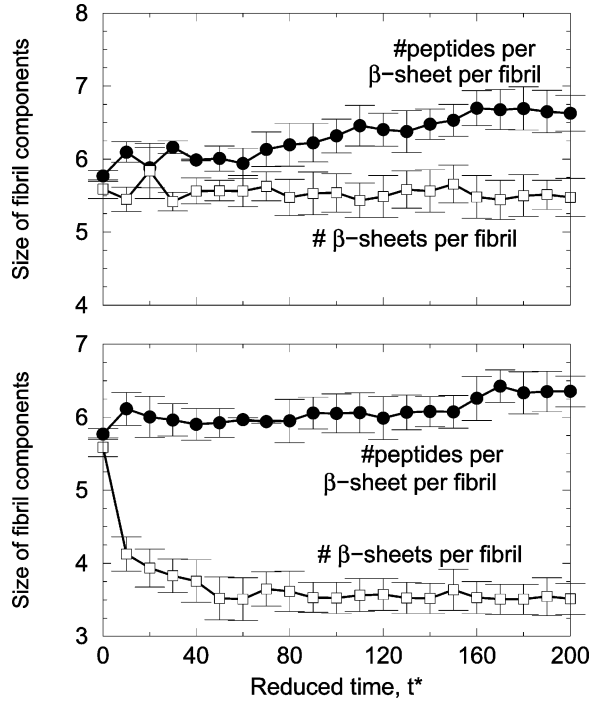

Figure 8. Average number of peptides per β-sheet in a fibril (●) and the average number of β-sheets per fibril (□) versus reduced time, t^*, for the 48-peptide system at $T^* = 0.15$ (top panel) and $T^* = 0.16$ (bottom panel). Results are from simulations starting with fibrils formed at $T^* = 0.11$ that are subsequently heated to the temperatures of interest.

systems at high temperatures ($T^* = 0.12-0.14$). Interestingly enough, the overall orientation of a β-sheet in our fibrils is different from that of the neighboring β-sheets; in fact, 61.6% (±5.2) of the β-sheets in our fibrils are arranged in an antiparallel orientation. This means that, within each β-sheet, peptides are parallel to one another; however, peptides within a β-sheet are antiparallel to peptides within the neighboring β-sheets. The end residues of neighboring peptides are usually aligned directly, i.e., in register. In-register parallel β-sheets are similarly observed in experiments on fibrils formed by β-amyloid proteins[129−131] and in a computer simulation study by Gsponer[32] on a three-peptide β-sheet formed by the heptapeptide GNNQQNY from the yeast prion Sup35. Further evidence for in-register parallel β-sheets comes from the work of Kuwata,[43] who performed both NMR-detected hydrogen bond exchange experiments and molecular dynamics simulations on a fibril-forming mouse prion protein fragment 106−126 and observed that parallel β-sheets stabilized by the central alanine-based residues VAGAAAAGAV are the most stable structures. The predominance of parallel pairing in our model differs from the results of a previous study by Ma and Nussinov[38] who examined the stability of proposed fibril structures by conducting nanosecond simulations at high temperatures on already-formed parallel and antiparallel fibril oligomers containing either AGAAAAGA or AAAAAAAA peptides and found that the antiparallel orientation is the most stable structure. Perhaps, the orientation of peptides in β-sheets depends on the peptide length. This is known to be the case for Aβ where Aβ(34−42)[132] and Aβ(16−22)[133] form antiparallel β-sheets, while Aβ(10−35) [100] and Aβ(1−40)[130] form parallel β-sheets. The dependency of the peptide orientation in β-sheets specifically and the formation of β-sheets or fibrils in general on the peptide length will be explored in a future publication. Each of the peptides in our fibrils is almost fully extended as indicated by its end-to-end distance and radius of gyration, which are 40.81 Å (±4.76) and 13.10 Å (±1.04) compared with 51.24 Å and 15.10 Å, respectively, for the completely stretched-out linear peptide conformation and 29.05 Å (±0.39) and 10.45 Å (±0.08), respectively, for the random-coil conformation.

The β-sheets in the fibrillar structures that result from our simulations are stabilized by intrasheet backbone−backbone hydrogen bonds running parallel to the length of the sheet. The adjoining β-sheets are held together by intersheet side chain−side chain hydrophobic interactions oriented nearly perpendicular to the length of the sheet. In addition, each β-sheet is stabilized by intrasheet hydrophobic interactions oriented parallel to the length of the sheet. These intrasheet hydrophobic contacts are a consequence of the tight packing in the complex and serve to lower the overall internal energy of the complex. The packing of our fibrillar structures mimics the close packed sheets found in experiments on a variety of peptides.[11,134,135] Our typical fibrillar complex is a dense, ordered structure with tightly packed side chains. The intrasheet (C_α to C_α) distance is 4.92 Å (±0.01), which is slightly higher than the experimentally determined value of 4.7−4.8 Å for close packed sheets of different peptides.[11,134,135] In addition, the intersheet (C_α to C_α) distance is 7.52 Å (±0.23), which is comparable to the low end of experimental values of 8−10 Å for transthyretin fragments[136] and significantly smaller than the experimentally determined value of ∼9−10 Å for close packed sheets of Alzheimer's peptides.[11,134,135] This is not surprising since both transthyretin fragments and β-amyloid peptides have big bulky side chains, whereas our model peptides consist mostly of alanine residues which have one of the smallest size side chains.

The β-sheets in the fibrillar structures are in a staggered arrangement along the fibril axis as similarly observed in polyalanine-rich domain in PrP.[137,138] A snapshot in Figure 9a of the 96-peptide fibrillar structure formed at $R = 1/10$, $c = 5.0$ mM, and $T^* = 0.13$ shows that when viewed from the side, each peptide within a particular β-sheet (e.g., green sheet in red circle) lies between two peptides of the neighboring β-sheets (e.g., dark blue sheet and purple sheet). In other words, each β-sheet is shifted along the fibril axis by ∼2.5 Å with respect to the neighboring β-sheets. In addition, when viewed down the fibril axis in Figure 9b, the alanine side chains on adjacent peptides within a particular β-sheet (e.g., green sheet in red

(129) Benzinger, T. L. S.; Gregory, D. M.; Burkoth, T. S.; Miller-Auer, H.; Lynn, D. G.; Botto, R. E.; Meredith, S. C. *Proc. Natl. Acad. Sci. U.S.A.* **1998**, *95*, 13407−13412.
(130) Antzutkin, O. N.; Balbach, J. J.; Leapman, R. D.; Rizzo, N. W.; Reed, J.; Tycko, R. *Proc. Natl. Acad. Sci. U.S.A.* **2000**, *97*, 13045−13050.
(131) Balbach, J. J.; Petkova, A. T.; Oyler, N. A.; Antzutkin, O. N.; Gordon, D. J.; Meredith, S. C.; Tycko, R. *Biophys. J.* **2002**, *83*, 1205−1216.
(132) Lansbury, P. T., Jr.; Costa, P. R.; Griffiths, J. M.; Simon, E. J.; Auger, M.; Halverson, K. J.; Kocisko, D. A.; Hendsch, Z. S.; Ashburn, T. T.; Spencer, R. G. S.; Tidor, B.; Griffin, R. G. *Nat. Struct. Biol.* **1995**, *2*, 990−998.
(133) Balbach, J. J.; Ishii, Y.; Antzutkin, O. N.; Leapman, R. D.; Rizzo, N. W.; Dyda, F.; Reed, J.; Tycko, R. *Biochemistry* **2000**, *39*, 13748−13759.
(134) Harper, J. D.; Lieber, C. M.; Lansbury, P. T., Jr. *Chem. Biol.* **1997**, *4*, 951−959.
(135) Jurnak, F.; Yoder, M. D.; Pickergill, R.; Jenkins, J. *Curr. Opin. Struct. Biol.* **1994**, *4*, 802−806.
(136) Jarvis, J. A.; Craik, D. J.; Wilce, M. C. *Biochem. Biophys. Res. Commun.* **1993**, *192*, 991−998.
(137) Inouye, H.; Kirschner, D. A. *Fibre Diffraction Review* **2003**, *11*, 102−112.
(138) Nguyen, J. T.; Inouye, H.; Baldwin, M. A.; Fletterick, R. J.; Cohen, F. E.; Prusiner, S. B.; Kirschner, D. A. *J. Mol. Biol.* **1995**, *252*, 412−422.

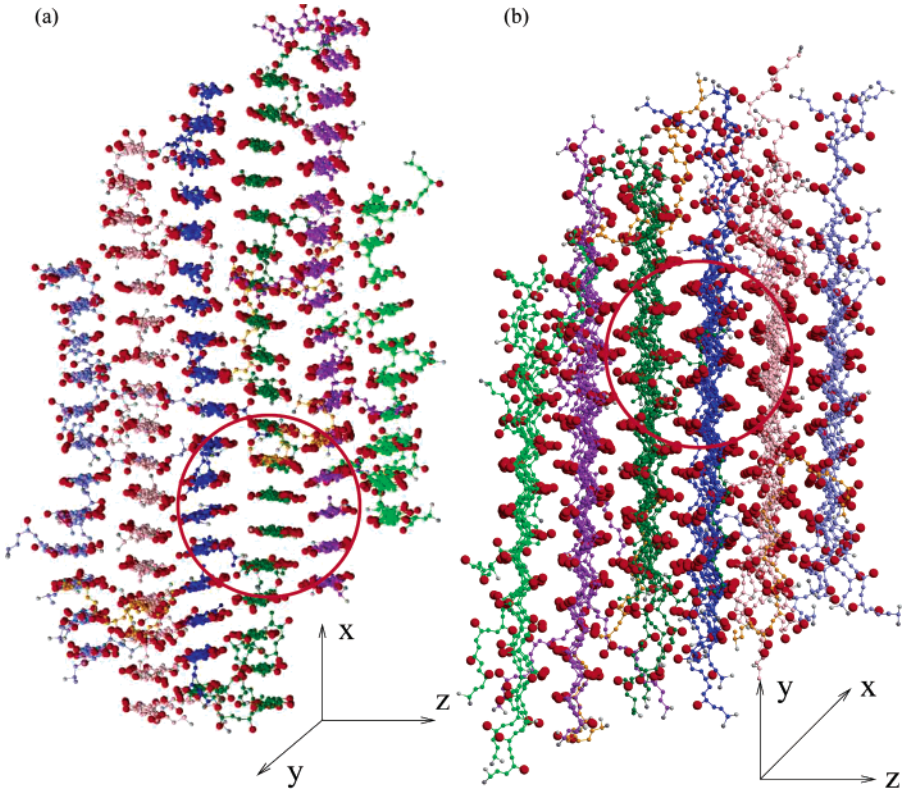

Figure 9. Snapshots of the 96-peptide fibrillar structure formed at $R = 1/10$, $c = 5.0$ mM, and $T^* = 0.13$. The fibrillar structure is viewed (a) from the side and (b) down the fibril axis. Note that the *x*-axis is in the intrasheet hydrogen bonding direction (i.e., fibril axis), *y*-axis is in the chain direction, and *z*-axis is in the intersheet direction. Hydrophobic side chains are red; backbone atoms of different peptides have different colors, assigned so that it will be easy to distinguish the various sheets. United atoms are not shown full size for ease of viewing.

circle) are aligned directly (stacked on top of one another in the figure) and alternate from one side of the sheet to the other. Alanine side chains on an adjacent sheet (e.g., dark blue sheet) also alternate from side to side but shift so that they fit into the "pocket" on a neighboring sheet.

Our fibrils contain the same number of β-sheets as in real fibrils, four to six sheets.[11,99−101] Snapshots of fibrils formed for different system sizes are shown in Figure 10. At $c = 5$ mM, $R = 1/10$, and $T^* = 0.13$, the fibrils formed from the 12-peptide system contain between two to three β-sheets, whereas the fibrils from the 24-peptide system contain between two to four β-sheets. At the same concentration, temperature, and hydrophobic interaction strength, the 48-peptide system forms fibrils containing between three to six β-sheets. When the system size is increased further to 96 peptides, the fibrils again contain between four to six β-sheets. This indicates that as the system size is increased significantly, the number of β-sheets asymptotes to a value near six. Once the fibrillar structure reaches its critical β-sheet number, monomeric peptides tend to attach to the fibrillar structure rather than creating an isolated β-sheet. The kinetics of bigger systems will be explored in a future publication.

There is an energetic explanation for the tendency of the fibrils to grow very long along the fibril axis rather than to grow laterally once the number of β-sheets within a fibril reaches six. First, there is an energetic preference for a peptide to attach itself to the end of a β-sheet within the fibril as opposed to the side of the fibril. Attaching to the end of the sheet would result in the formation of 15 hydrogen bonds and 27 hydrophobic interactions, while attaching to the side of the fibril would result in the formation of only 26 hydrophobic interactions. Second, there is an energetic preference for a peptide to attach itself to the end of a β-sheet within a fibril as opposed to attaching itself to another isolated peptide to form a β-sheet. The latter case would result in the formation of 13 hydrophobic interations less than the former case. Last, we believe that although there is an entropic preference for forming additional separate β-sheets, this preference is negligible once the surface area at the end of the fibril is large enough for the peptide to land. In addition, peptides at the end of fibrils are already in the β-strand conformation, which creates a relatively large bed of hydrogen-bonding atoms that stick out and line up. They are thus readily available and receptive to forming hydrogen bonds with an incoming peptide.

Fibril Formation as a Function of the Hydrophobic Interaction Strength between Nonpolar Side Chains. The strength of the hydrophobic interaction between nonpolar side chains plays an important role in fibril formation as indicated in Figure 11, which displays the percentage of peptides in (a) fibrillar and (b) β-sheet structures as a function of temperature for the $c = 5$ mM system at different ratios, $R \equiv \epsilon_{HP}/\epsilon_{HB}$, of the strength of the hydrophobic interaction relative to that the hydrogen bond. As the strength of the hydrophobic interaction increases from $R = 1/10$ to $R = 1/8$, the percentage of peptides in fibrils slightly decreases at all temperatures as seen in Figure 11a. But as the strength of the hydrophobic interaction increases from $R = 1/8$ to $R = 1/6$, the percentage of peptides in fibrils decreases dramatically at all temperatures. Instead, the system at $R = 1/6$ forms amorphous aggregates. The average number of interpeptide hydrophobic interactions is 52% greater in amorphous aggregates than in fibrils, while the number of

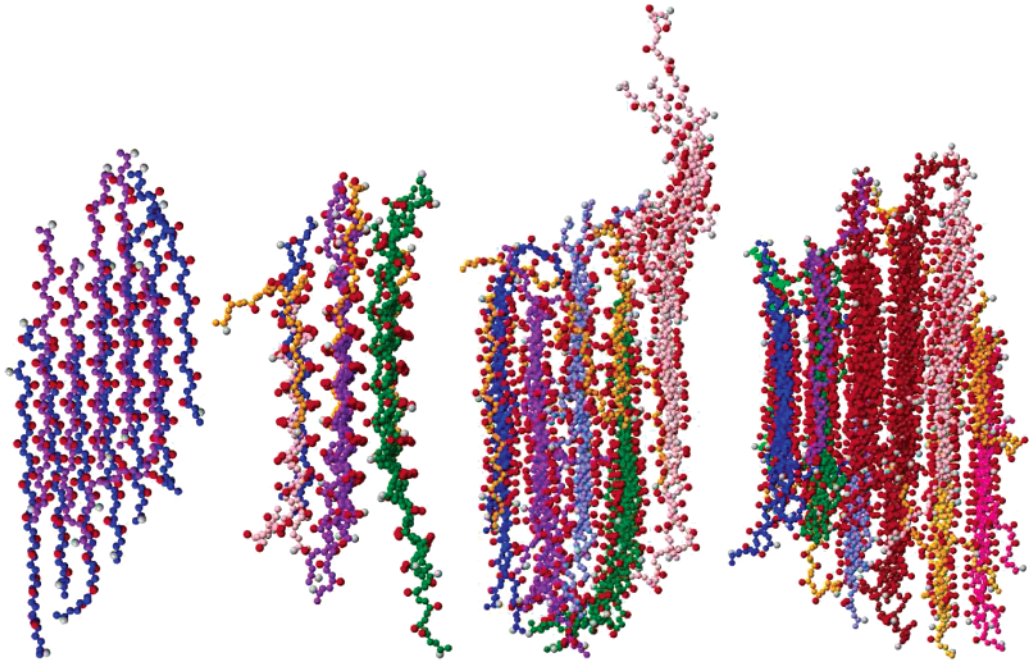

Figure 10. Snapshots of fibrillar structures formed at different system sizes at $R = 1/10$, $c = 5.0$ mM, and $T^* = 0.13$. Hydrophobic side chains are red; backbone atoms of different peptides have different colors, assigned so that it will be easy to distinguish the various sheets. United atoms are not shown full size for ease of viewing.

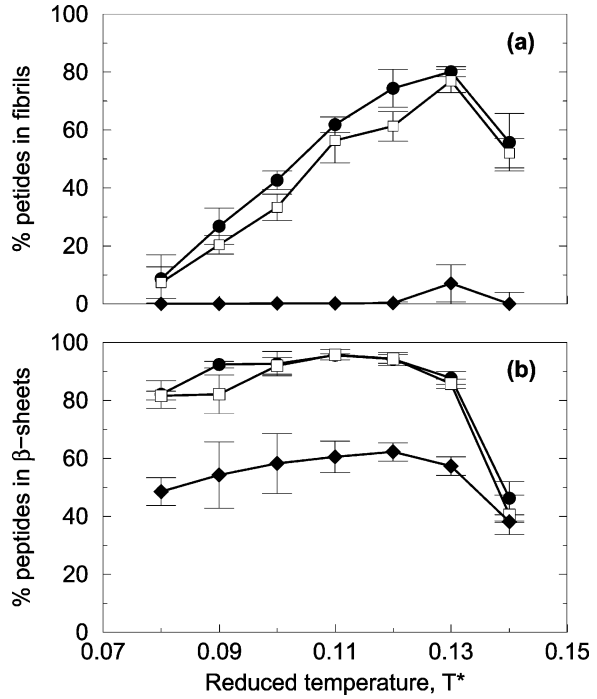

Figure 11. Percentage of peptides in (a) fibrillar structures and (b) β-sheet structures at concentration $c = 5$ mM versus temperature at three ratios R of the strength of the hydrophobic interaction relative to that of the hydrogen bond: $R = 1/10$ (●), $R = 1/8$ (□), and $R = 1/6$ (◆).

interpeptide hydrogen bonds is 35% less in amorphous aggregates than in fibrils (data not shown). This indicates that having a large hydrophobic interaction strength essentially overwhelms the system, forcing it to form more hydrophobic interactions than hydrogen bonds and hence favoring the formation of amorphous aggregates. This is similarly observed in a simulation study on the folding of different polypeptide chains of different lengths by Knott and Chan[95] who observed that the peptides undergo hydrophobic collapse into compact conformations with little secondary structure content.

Fibril formation seems to be more sensitive than β-sheet formation to the strength of the hydrophobic interaction between nonpolar side chains as can be seen by comparing the results in Figure 11a and 11b. Although there are no fibrils formed at $R = 1/6$, about half of the peptides form β-sheets which are intertwined in large aggregates. However, unlike the fibrils, whose average β-sheet size is about seven peptides (data not shown), these β-sheets are relatively small, each containing approximately two peptides (data not shown). These β-sheets are twisted around each other to maximize the number of hydrophobic interactions, as discussed above.

Limitations. It is important to point out that our model and analysis are subject to a number of limitations. First, we do not include charged residues at the ends of the model peptide chains, which have been shown to be important in experimental systems for reducing amorphous aggregation and precipitation. Second, it is possible that a more elaborate model force field is required to adequately represent peptides and their environment. Specifically, we have neglected solvent effects by incorporating solvent as a potential of mean force which has an equal effect on all united atoms regardless of the chain conformation. Consequently united atoms in the interior of a compact structure are just as affected by solvent as if they were fully exposed in a random coil structure. A more accurate solvation model would allow forces, such as the hydrogen bonding force in the core of a collapsed chain or an aggregate, to be different from those at the surface. In addition, we have fixed the strengths of the hydrogen bond and hydrophobic interactions, making them independent of temperature. Dill[139] and Chan[140] have proposed

(139) Dill, K. A.; Alonzo, D. O. V.; Hutchinson, K. *Biochemistry* **1989**, *28*, 5439−5449.

a temperature-dependent hydrophobic potential that undergoes a maximum at intermediate temperatures, accounting for weakened interactions from cold denaturation at low temperature and from heat denaturation at high temperature.[139] Further simulation studies with our model will be required to probe the importance of temperature-dependent interactions. Third, the hydrophobic interaction needs to be between 1/10 and 1/8 the magnitude of the hydrogen-bond potential in order for fibrillization to occur, whereas the experimental ratio is closer to at least a third.[95] We think that if the hydrophobic interaction were higher, we would get fibrils eventually, but we would have to wait a very long time while the system figures out how to get out of kinetic traps. So we are essentially speeding up the calculation by looking at low values of the hydrophobic interaction. We are doing the same thing when we look at systems at high concentrations. Because of these limitations, we are not comfortable introducing temperature and energy scaling factors to compare our results directly with those observed in experiments. Thus our results are meant to be interpreted qualitatively rather than quantitatively.

Conclusions

Computer simulations offer unique opportunities to observe and analyze molecular-level events in protein systems that are difficult or impossible to observe experimentally. In simulating large multipeptide systems using an intermediate resolution protein model in conjunction with the discontinuous molecular dynamics, we have been able to observe the formation of fibrils containing polyalanine peptides starting from random coils. We find that there is a strong relationship between the formation of α-helices, β-sheets, aggregates, and fibrils and the environmental conditions such as temperature, concentration, and hydrophobic interaction strength. At low peptide concentrations, random-coil peptides form α-helices at low temperatures and revert to random-coil conformations at high temperatures. When the concentration is increased slightly to intermediate values, random-coil peptides assemble into α-helices at low temperatures and large β-sheet structures at high temperatures. As the concentration is increased further to relatively high values, random-coil peptides form β-sheets over a wide range of temperatures; these β-sheets assemble into fibrils at temperatures above a critical temperature that decreases with concentration. Fibrils are stable at temperatures above those at which the α-helical model peptides are stable. At very high temperatures and all concentrations, the system is in a random-coil state. These results agree qualitatively with the experimental results of Blondelle on $Ac-KA_{14}K-NH_2$ peptides.[87,88] They observed monomeric α-helical structures at 100 μM and 25 °C. As the peptide concentration increased to 1 mM, they found that β-sheet complex formation increased with increasing temperature, exhibiting an S-shaped dependence of temperature with a critical temperature of 65 °C. As the peptide concentration increased to 1.8 mM, they found that the critical temperature at which β-sheets start to form decreased to 45 °C.

The fibrils observed in our simulations mimic the structural characteristics observed in experiments in that most peptides within a β-sheet in our fibrils are highly parallel to one other[129−131] and moderately antiparallel to peptides within neighboring β-sheets, the intrasheet (C_α to C_α) distance is 5.05 Å (±0.07) (compared to experimental values of 4.7−4.8 Å[11,134,135]), the intersheet (C_α to C_α) distance is 7.52 Å (±0.23) (compared to experimental values of 8−10 Å[11,134−136]), and our fibrils contain about six β-sheets with each containing multiple peptides.[11,99−101] Finally, we find that when the strength of the hydrophobic interaction between nonpolar side chains is high compared to the strength of the hydrogen bond interaction, amorphous rather than fibrillar aggregates are formed.

Based on this initial success in simulating the formation of fibrils, we expect that computer simulations can assist in the identification of sources of aggregate stability, information vital to the rational design of therapeutic strategies in protein aggregation diseases. It is also likely that computer simulation studies will lead to a better understanding of the fundamental mechanisms of aggregate formation, permitting a clearer picture of aggregate involvement in the pathology of amyloid diseases.

Acknowledgment. The authors are grateful to Sylvie Blondelle, Ken Dill, Angel Garcia, Jeffery Kelly, Hideyo Inouye, Ron Wetzel, and Dan Kirschner for helpful discussions. This work was supported by the National Institutes of Health under Grant Number GM-56766 and the National Science Foundation under Grant Number CTS-9704044.

JA0539140

(140) Shimizu, S.; Chan, H. S. *J. Chem. Phys.* **2000**, *113*, 4683−4700.